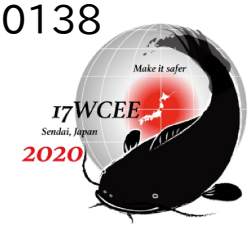

17th World Conference on Earthquake Engineering, 17WCEE
Sendai, Japan - September 13th to 18th 2020

EVALUATION OF THE PERFORMANCE OF DEEP, SLENDER COLUMNS THROUGH THE USE OF SUB-ASSEMBLIES

C. Flores Carreras[(1)], O. Sediek[(2)], J. McCormick[(3)], S. El-Tawil[(4)]

[(1)] *Graduate Student, University of Michigan, Ann Arbor, MI, USA, florcarr@umich.edu*
[(2)] *Graduate Student, University of Michigan, Ann Arbor, MI, USA, osediek@umich.edu*
[(3)] *Associate Professor, University of Michigan, Ann Arbor, MI, USA, jpmccorm@umic.edu*
[(4)] *Professor, University of Michigan, Ann Arbor, MI, USA, eltawil@umich.edu*

Abstract

After the 1994 Northridge and 1995 Hyogo-ken Nanbu earthquakes, engineers in the US began to favor the use of deep, slender columns in steel moment resisting frames over stockier wide flange sections as a means of satisfying the revised design requirements that emerged from the SAC Steel Project (more stringent drift limits, strong column-weak beam criteria, balanced panel zone design). Although deep, slender wide flange column sections tend to reduce drift due to their large moment of inertia, their local slenderness ratios also are larger and their radius of gyration about the weak axis is smaller compared to more traditional stockier wide flange columns. As a result, deep, slender wide flange columns are more prone to local buckling and out-of-plane global failure modes, raising concerns regarding their seismic performance. Previous member-level studies of deep wide flange columns under combined axial and lateral loads have identified an interaction between local and global instabilities. This interaction in some cases cause sections that currently meet the highly ductile seismic criteria to exhibit poor ductility, thereby increasing the potential for collapse. To explore and better understand these unexpected interactions between local and global instabilities in the presence of other building elements (beams and connections), a computational study is undertaken considering an interior column sub-assembly which features a wide flange column with wide flange beams. The sub-assemblies are obtained from different model building frames chosen to represent different column section sizes utilized in practice. The sub-assemblies are studied with combined axial and cyclic lateral loading protocols considering both symmetric and earthquake-consistent cycles. The constant applied axial load varies between twenty and forty percent of the column's yield strength. The performance of the sub-assemblies, and in particular the columns, is evaluated with respect to maximum moment capacity, moment capacity degradation with continued cycling, and ability to meet current seismic ductility requirements for moment frame systems. This investigation into the behavior of deep, slender wide flange columns provides valuable insight into the extent to which the interaction between local and global buckling modes are a concern in regards to the resiliency of steel moment resisting frames.

Keywords: Deep columns; Local buckling; Global buckling; Finite element; Sub-assembly modeling

1. Introduction

The 1994 Northridge and 1995 Hyogo-Ken Nanbu (Kobe) earthquakes exposed a great deal of vulnerabilities in the design and construction of steel moment resisting frames. Specifically, many steel buildings suffered damage due to improperly detailed connections that led to fracture near the complete joint penetration welds between the beam flanges and the column [1]. As a direct response to uncovering these issues, the SAC Steel Project was created to investigate and address the performance concerns of steel moment frames [2]. The seismic provision changes that originated from this investigation (more stringent drift limits, strong column-weak beam criteria, balanced panel zone design) solved a lot of the issues that were discovered, but also made satisfying design requirements more difficult, pushing engineers towards deeper, more slender wide flange column sections. Although these deep, slender sections have the benefits of larger moments of inertia than stockier sections, they are more prone to local buckling and out-of-plane global failure modes due to larger local slenderness ratios and a smaller radius of gyration around their weak axis, respectively. Due to this fact, the use of deep, slender wide flange columns in steel special moment frames (SMF) has raised concerns regarding their expected performance during a seismic event.

Recent member-level studies of deep, slender wide flange columns have revealed previously unrecognized interactions between local and global instabilities that result in many deep columns failing to deliver adequate plastic rotation capacity when subjected to high axial loads and bending moments [3]. Further investigations are needed into these interactions, specifically in the presence of other building elements such as beams and connections, to understand the extent to which they influence the column and frame behavior. To this end, this paper presents a computational study of four sub-assemblies that feature either a wide flange or hollow structural section (HSS) column and a typical beam to column seismic moment connection.

2. Building Archetypes

The model building frames from which the sub-assemblies are obtained are based on those presented in NIST [4] and were all designed following the AISC seismic provisions [5] and ASCE seismic design requirements [6]. The configuration for all of the SMF archetypes consists of a rectangular building plan with a three-bay perimeter moment frame on each side (Fig. 1a). For the purpose of this study, three different sub-assemblies are used to span the range of stocky to deep wide flange column sections. An additional sub-assembly is included which features an HSS column section to study the difference in performance with a comparable wide flange section. Table 1 lists the selected sub-assemblies with other relevant information such as the building height for the building from which the sub-assembly was extracted. All sub-assemblies represent a first story interior column that extends up to its inflection point in the second story. Further details on the design process and complete information on the model building frames can be found in NIST [4].

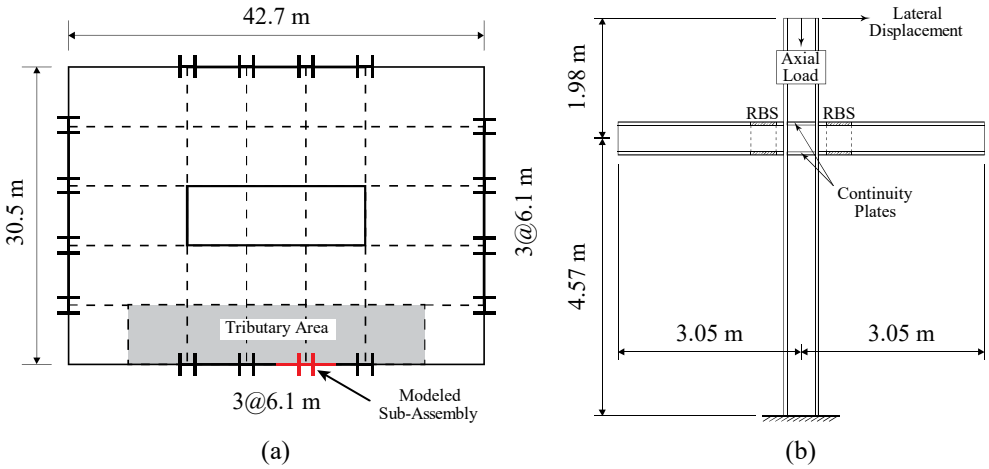

Fig. 1 – (a) Typical building plan configuration and (b) schematic of the wide flange column sub-assembly

Table 1 – List of modeled sub-assemblies

Sub-assembly	Column Section (mm, mm×kg/m)	Beam Section (mm×kg/m)	Axial Load Range	Building Stories
S1	HSS508×203.2×15.9	W530×85	(0.2 - 0.4) P_y	4
S2	W360×110	W410×85		4
S3	W610×153	W530×109		4
S4	W920×449	W760×161		20

Sub-assemblies S2 through S4 featured a wide flange column connected to two wide flange beams in a cruciform configuration (Fig. 1b). The connection was a typical reduced beam section (RBS) seismic moment connection designed according to AISC 358-05 [4, 7]. The HSS column section in sub-assembly S1 was selected through an iterative design process considering a similar building frame layout to the one from which S3 was extracted. Because there are no prequalified HSS column-to-wide flange beam seismic moment connections, the connection for sub-assembly S1 is modeled based on the RBS diaphragm connection presented in Vulcu et al. [8]. Details in regards to this connection are shown in Fig. 2. The connection was originally developed for concrete-filled HSS columns connected to wide flange beams and was experimentally shown to perform adequately under cyclic lateral loading, exhibiting a rotation capacity of over 4% drift [8]. The connection uses external diaphragm plates and vertical column stiffeners to connect the beams to the column and transfer the loads to the sidewalls of the HSS column. While these experiments were done with a concrete-filled HSS column, a subsequent computational study also showed the RBS diaphragm connection performed similarly in the absence of concrete-fill [9].

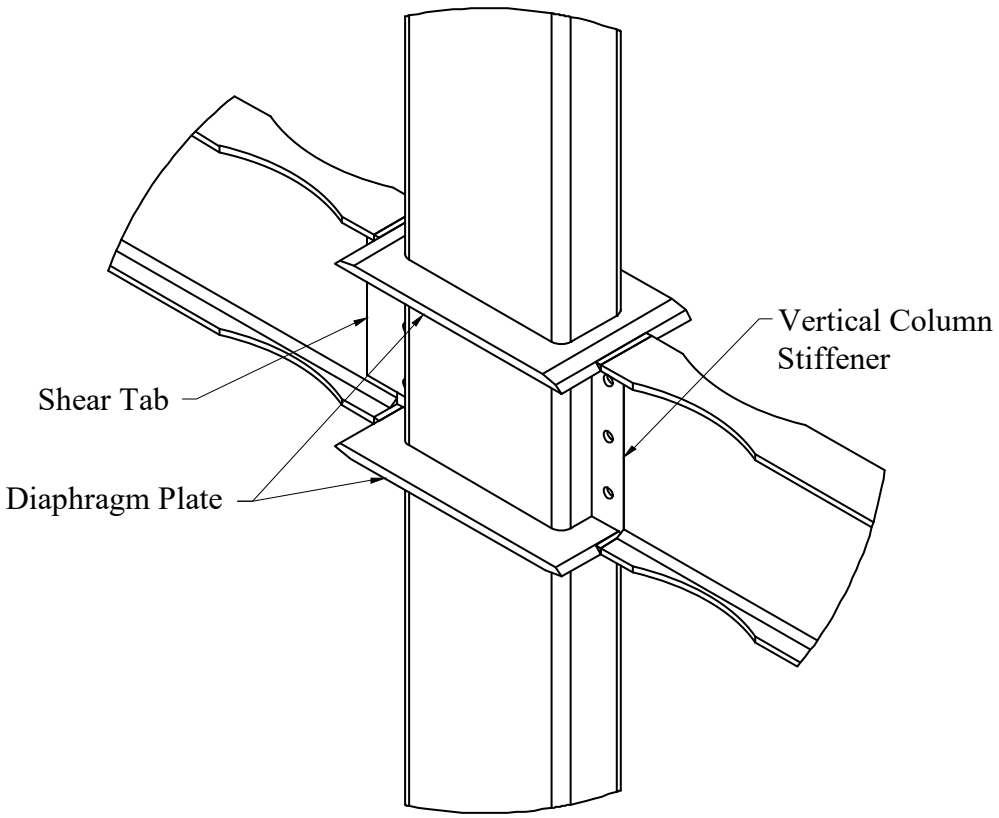

Fig. 2 – HSS column-to-wide flange beam RBS diaphragm moment connection details

3. Modeling approach

A full-scale finite element model of each cruciform sub-assembly is created in the finite element software Abaqus 2017 [10] (Fig. 3). The sub-assembly consists of a first floor column member with two beams connected to the opposing flanges of the column. The distance between the column centerline and the beam ends corresponds to half of the bay width and represents the expected inflection point in the beam under lateral loading. The distance between the fixed base of the column and the center of the beam-to-column connection corresponds to the first floor story height of the model building frames. An additional 1.98 m of column height, corresponding to half of the second story height, is also included in order to have realistic boundary conditions for the beam-to-column connection. The top of the column is where both the axial and lateral loads are applied, and otherwise has no additional boundary conditions. The boundary conditions at the beam ends consist of a roller support that allows rotation and movement in plane. These end conditions are used to represent the anticipated inflection point in the column and beams. An additional constraint is added to tie the vertical degree of freedom at the beam ends to the displacement at the top of the column. This constraint is established through an equation constraint that ensures both displacements are always equal. By applying this additional constraint, the finite element model is accounting for the fact that axial shortening has been observed in columns under large axial loads and bending moments.

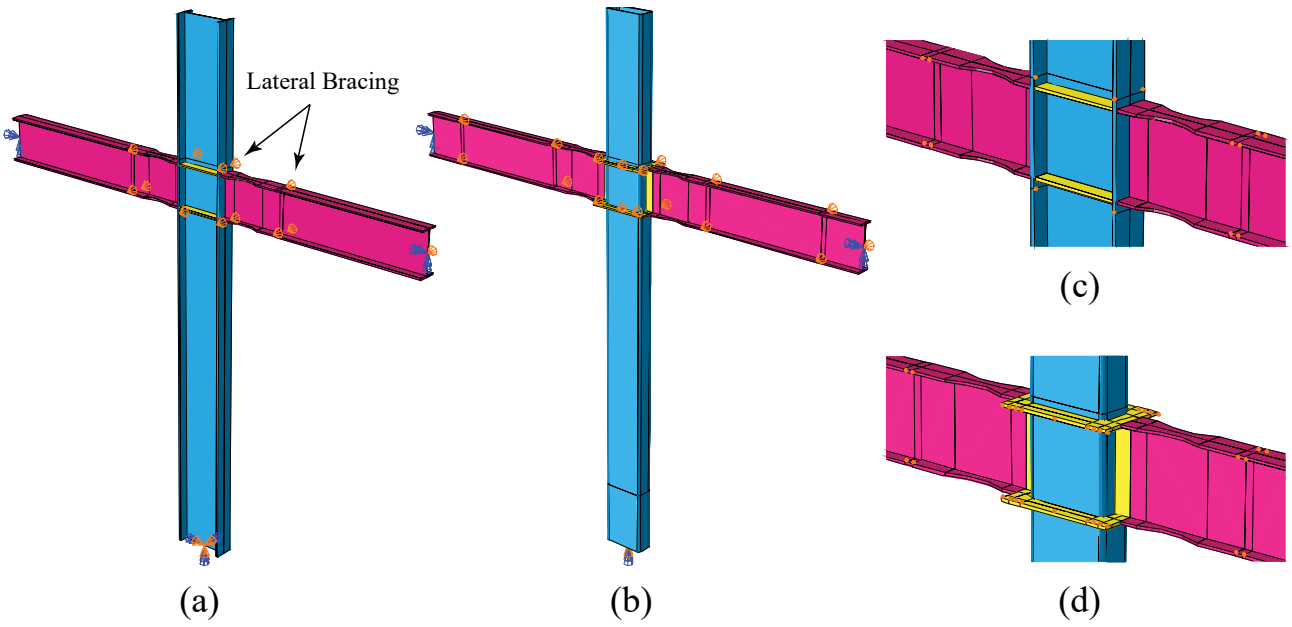

Fig. 3 – Finite element model of the (a and c) wide flange column and (b and d) HSS column sub-assemblies

3.1 Material and model details

The different steel grades that are used in the sub-assemblies are ASTM A992 (F_y = 345 MPa, F_u = 448 MPa), ASTM A500 Gr. B (F_y = 317 MPa, F_u = 400 MPa), and ASTM A572 Gr. 50 (F_y = 345 MPa, F_u = 448 MPa) for the wide flange members, HSS column, and steel plates, respectively. The ASTM A992 material model is a nonlinear kinematic hardening model with two back stress terms. The calibration of this model is done by developing a true stress-true strain curve and comparing it to the material model proposed by Arasaratnam et. al. [11]. More details on the calibration and validation of this material model are presented in Wu et. al. [12]. The ASTM A500 material model utilizes a combined kinematic and isotropic hardening law. Different hardening parameters for this material are also specified for the flats and corners of the section to take into account the effects of cold working. In general, cold working results in the corners of the HSS having a higher yield strength, but lower ductility when compared to the flats. A more in-depth discussion of this topic is

presented in Fadden and McCormick [13]. The kinematic and isotropic material parameters are calibrated using experimental data from coupon specimens and the moment-rotation curves from cantilever HSS beam members undergoing cyclic displacements [14]. Finally, the material model for ASTM A572 Gr. 50 steel is an isotropic hardening model based on experimental coupon data.

The sub-assemblies are constructed using S4R elements (4-node doubly curved shell, reduced integration, hourglass control) with an element size of 19.1 mm along the column, connection, and RBS regions in the beam. An element size of 38.1 mm is used everywhere else. Initial deformations are applied to the finite element model of the column in the column base region in order to accurately capture local buckling during the simulation. The shape of the initial deformations is obtained through a column buckling analysis. For the case of the HSS column, the magnitude of the imperfection is scaled to half of the maximum allowable imperfection prescribed by the ASTM standard for cold-formed tubular shapes [15]. For the case of the wide flange column, the magnitude is scaled to the smaller value between $b_f/250$ and $h_w/250$. Following the AISC Seismic Provisions' [16] requirements for SMF systems, lateral bracing of the sub-assembly is provided by constraining the out-of-plane displacement at the beam-to-column connection region, near the RBS protected zone, and at appropriate locations along the beams. A self-contact interaction is applied at the column base region of the sub-assemblies to take into account possible squashing at high drifts. Fracture is not considered.

3.2 Loading

Various levels of constant column axial load are used to study their effect on the overall strength and seismic performance of the sub-assemblies. The axial load range considered is from $0.2P_y$ to $0.4P_y$ in increments of $0.05P_y$, where P_y is the column axial yield load calculated using the nominal section area and the yield strength obtained from coupon tests of either the ASTM A992 or ASTM A500 Gr. B steel. The two lateral loading protocols used in this study are shown in Fig. 4. The symmetric cyclic (SC) loading protocol is the one prescribed by the AISC Seismic Provisions [16] for prequalifying seismic moment connections and consists of a sequence of fully reversed, continually increasing drift levels that go from 0.00375 rad. to 0.08 rad. The cyclic ratcheting (CR) protocol was developed by Wu et. al. [12] and represents a collapse-consistent progression of drift levels that incorporate ratcheting behavior up to 0.04 rad. after the initial symmetric cycles. The CR protocol was only applied to the sub-assemblies with an axial load of $0.3P_y$.

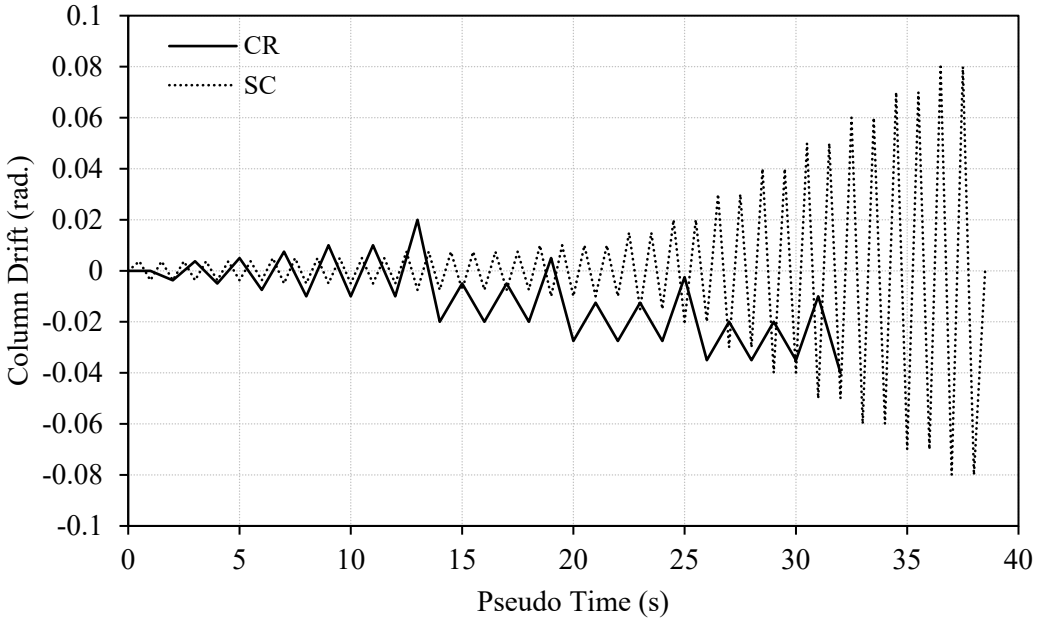

Fig. 4 – Loading protocols used in the finite element study

4. Results

4.1 Effects of axial load (SC protocol)

Varying the axial load on the column has a significant effect on the cyclic performance of each sub-assembly in terms of maximum moment capacity, moment capacity degradation with continued cycling, and overall stability. In terms of the column's maximum moment capacity, all of the wide flange column sub-assemblies experience a similar rate of decrease in moment capacity as the axial load ratio increases (Fig. 5a). However, the sub-assembly with the HSS column shows the least amount of decrease in its overall moment capacity as the axial load increases to $0.40P_y$. Figure 5b and 5c show the column's moment capacity degradation from the overall maximum moment capacity to the moment capacity at the 2% and 4% inter-story drift levels. At 2% drift, sub-assembly S2, which represents the stockier pre-Northridge wide flange column, exhibits no moment capacity degradation for all axial load ratios and sub-assembly S1 only shows degradation at the 0.35 and 0.40 axial load ratios. Conversely, the sub-assemblies with deep wide flange columns, S3 and S4, experience moment capacity degradation at the 2% drift level for every axial load ratio with S3 having degraded 50% and 73% at $0.35P_y$ and $0.40P_y$, respectively. The magnitude of this degradation is significantly high for an SMF at this drift level. Considering the sub-assemblies' performance out to the 4% drift level, some of the simulations become too unstable and abort prior to reaching the first cycle to 4% drift. This behavior is typically associated with a moment capacity nearing zero. Therefore, it is reasonable to assume the structure is nearing collapse due to loss of axial and lateral load carrying capacity. Specifically, sub-assemblies S3 and S4, which represent the sub-assemblies with deep column sections, do not manage to reach 4% inter-story drift with an axial load of $0.30P_y$ and $0.40P_y$, respectively, and show significantly higher moment capacity degradation at lower axial load ratios (Fig. 5c).

As mentioned previously, although the section sizes in sub-assembly S1 (HSS column) are selected to be comparable in strength to S3, S1 exhibits a different behavior due to the presence of the HSS column. At 4% drift, S1 exhibits lower moment capacity degradation compared to S3 at all axial load levels (Fig. 5c). As shown in Fig. 6b and 6d, this difference in performance can be attributed to the wide flange column undergoing more local buckling at the same rotation level. In the case of S1, after significant local buckling occurs at the base of the column, the column starts to undergo shortening. As a result, self-contact interaction is observed which affects the overall behavior of the sub-assembly (Fig. 6a). Because fracture is not considered in the models, it is likely that this behavior is not accurate at higher rotation levels (more than 0.06 rad.) where fracture initiation has been observed in the corners of HSS members during previous testing [17].

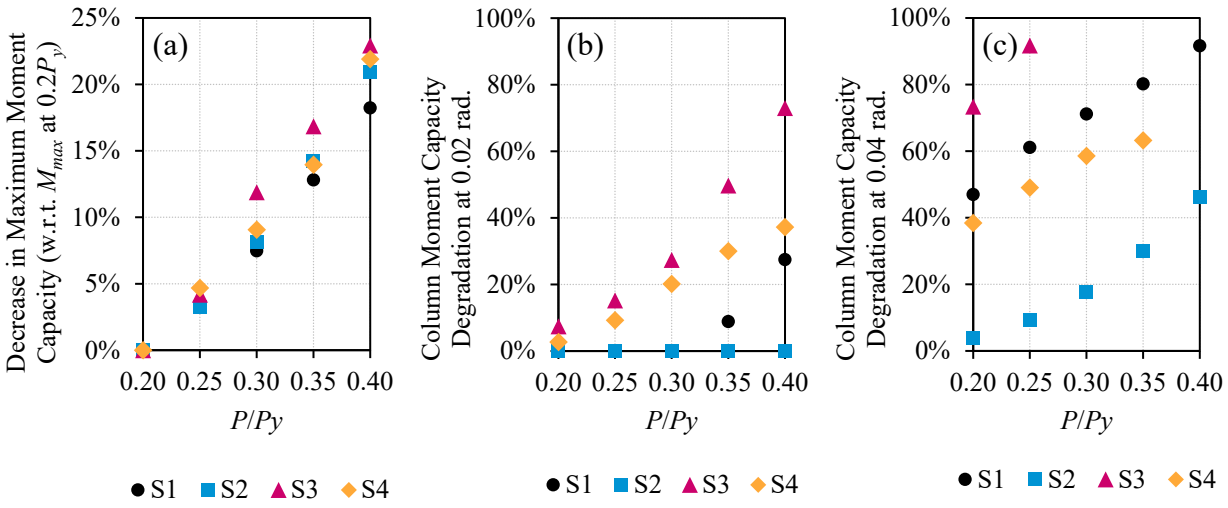

Fig. 5 – (a) Percent decrease in column maximum moment capacity with respect to M_{max} at $0.2P_y$. (b and c) Column moment capacity degradation at 0.02 rad. and 0.04 rad., respectively. SC protocol

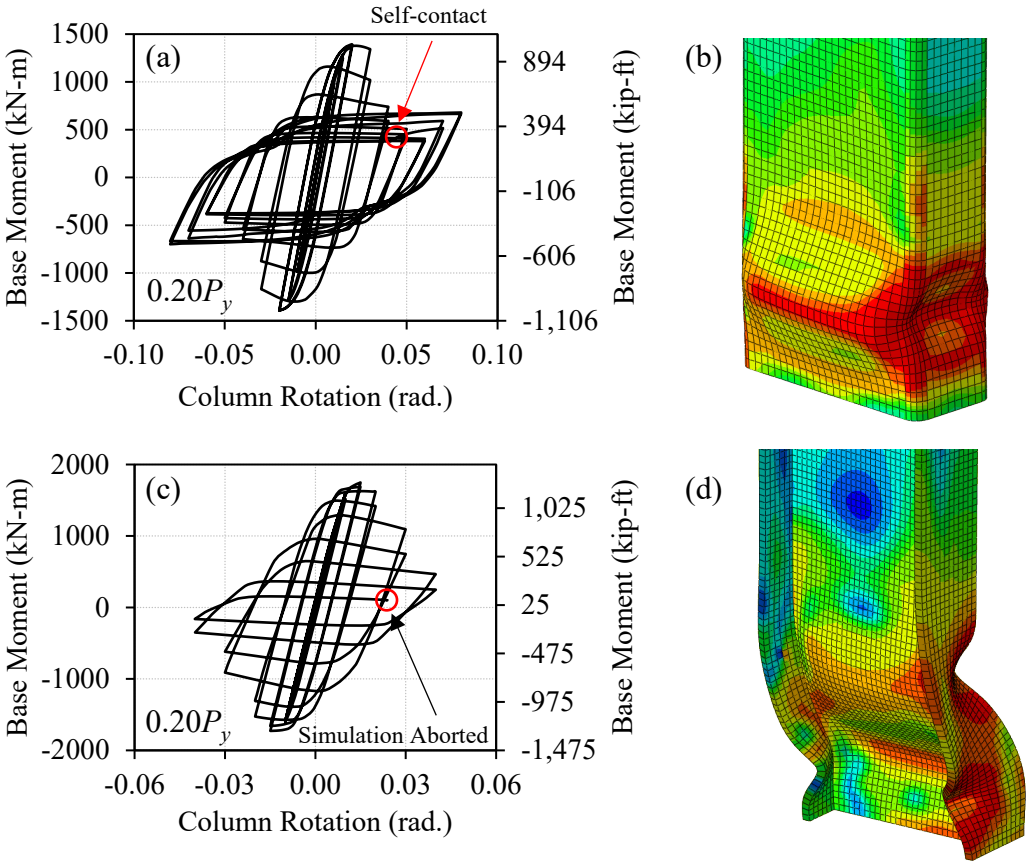

Fig. 6 – (a and c) Moment-rotation behavior for S1 and S3, respectively. (b and d) Local buckling at column base during the first 4% inter-story drift cycle for S1 and S3, respectively. SC protocol

4.2 Effect of loading protocol

As shown in Fig. 7, there are significant differences in performance when comparing the SC and CR loading protocols. In general, the SC protocol places larger demands on the sub-assembly and does not account for the ratcheting effect often seen in collapse scenarios. The S3 sub-assembly does not reach the first 0.04 rad. cycle when subject to an axial load ratio of 0.30 under the SC protocol. However, under the CR protocol it is able to survive the whole protocol with the same axial load level. The main reason for the difference in performance is the amount of observed local buckling as seen in Fig. 7b and 7d. Because the SC protocol consists of fully reversed cycles, the local buckling of both flanges of the column at the column base is much more significant, while in the CR protocol most of the local buckling is concentrated in one of the flanges due to cyclic ratcheting not allowing the column to bend in the opposite direction. As a result, the columns in the sub-assemblies that underwent the SC protocol experience considerably larger deformations and subsequent loss in moment capacity and axial load carrying capacity resulting in poorer cyclic performance when compared to its CR counterpart. Similar results are observed across all four sub-assemblies. These results suggest that it is important to consider multiple loading scenarios as some cases may be overly demanding and result in an exaggerated poor behavior.

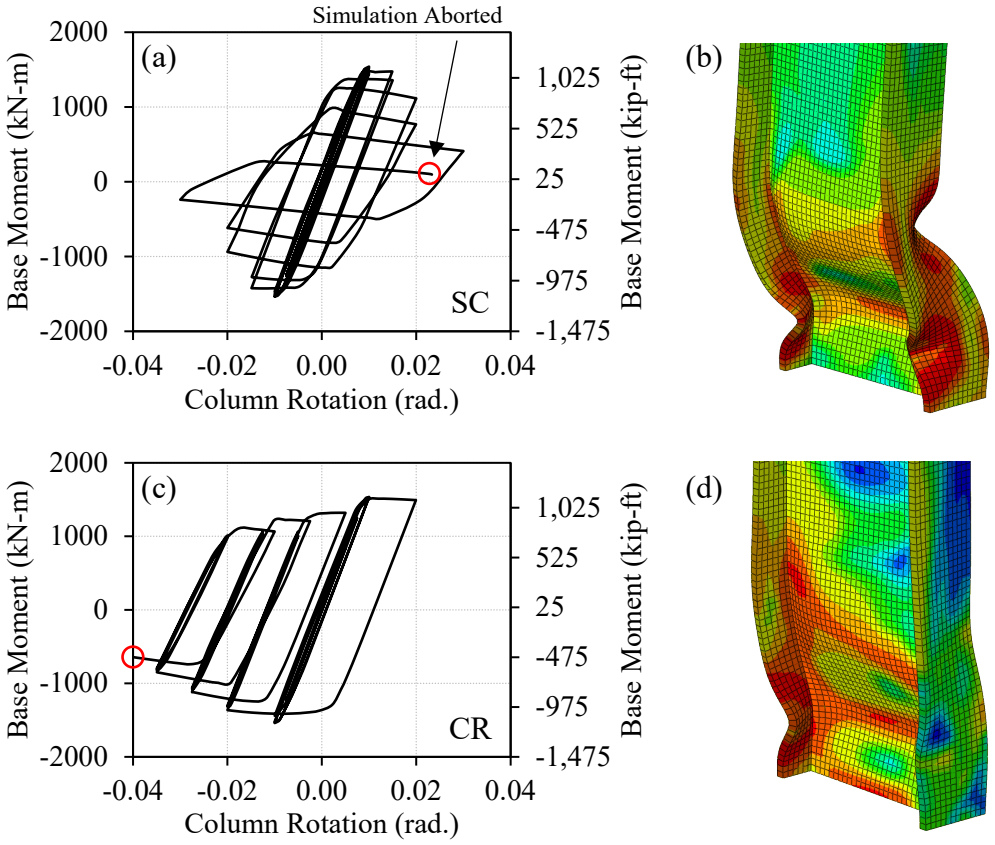

Fig. 7 – (a and b) S3 column base moment, SC protocol, $0.30P_y$, 2nd 3% drift cycle. (c and d) S3 column base moment, CR protocol, $0.30P_y$, 4% drift

5. Conclusions

A computational study is conducted on four steel cruciform sub-assemblies subjected to high axial and lateral loads. Multiple constant axial load levels and two different lateral loading protocols are considered. The results from the finite element analyses showcase how deep, slender wide flange columns that currently meet SMF requirements do not necessarily perform as expected and can exhibit poor ductile behavior, in many cases not being able to reach 4% inter-story drift. The deeper wide flange columns also sustain more severe loss in moment capacity with continued cycling due to the interaction between local and global buckling. The HSS column performs better than a comparable wide flange column, consistently exhibiting less moment capacity degradation and reaching 4% drift at all axial load levels. The results show that the sub-assembly featuring the stockiest column section performs best and maintains both bending and axial load capacity out to 4% inter-story drift. Overall, the results from this study suggest deep, slender wide flange columns can have trouble meeting current seismic design standards when subjected to combined axial and lateral loads. These results agree with previous member level studies that have been conducted.

6. Acknowledgements

This research is supported by the financial assistance award 70NANB171TZ91 from the U.S. Department of Commerce, National Institute of Standards and Technology. Any opinions, findings, conclusions and recommendations expressed in this paper are those of the authors and do not necessarily reflect the views of the sponsor.

7. References

[1] Fadden MF (2013): Cyclic Bending Behavior of Hollow Structural Sections and their Application in Seismic Moment Frame Systems. *University of Michigan*.

[2] SAC Steel Project (2000): Loading Histories for Seismic Performance Testing of SMRF Components and Assemblies. *Report No. SAC/BD-00/10*.

[3] Uang C-M, Ozkula G, Harris J (2015): Observations from Cyclic Tests on Deep, Slender Wide-Flange Structural Steel Beam-Column Members. *Proceedings of the Annual Stability Conference*.

[4] NIST (2010): Evaluation of the FEMA P-695 Methodology for Quantification of Building Seismic Performance Factors. *NIST GCR 10-917-8*, Gaithersburg, Maryland.

[5] AISC (2005): Seismic Provisions for Structural Steel Buildings. *ANSI/AISC 341-05*, Chicago, Illinois.

[6] ASCE (2005): Minimum Design Loads for Buildings and Other Structures. *ASCE/SEI 7-05*, Reston, Virginia.

[7] AISC (2005): Prequalified Connections for Special and Intermediate Steel Moment Frames for Seismic Applications. *ANSI/AISC 358-05*, Chicago, Illinois.

[8] Vulcu C, Stratan A, Ciutina A, Dubina D (2017): Beam-to-CFT High Strength Joints with External Diaphragm. I: Design and Experimental Validation. *Journal of Structural Engineering*, **143**(5).

[9] Vulcu C, Stratan A, Ciutina A, Dubina D (2017): Beam-to-CFT High-Strength Joints with External Diaphragm. II: Numerical Simulation of Joint Behavior. *Journal of Structural Engineering*, **143**(5).

[10] Abaqus 2017 [Computer software]. *Dassault Systèmes Simulia Corporation*, Johnston, Rhode Island.

[11] Arasaratnam P, Sivakumaran KS, Tait MJ (2011): True stress-true strain models for structural steel elements. *ISRN Civ. Eng*, 1-11.

[12] Wu T-Y, El-Tawil S, McCormick P (2018): Highly Ductile Limits for Deep Steel Columns. *Journal of Structural Engineering*, **144**(4).

[13] Fadden M, McCormick J (2014): Finite element model of the cyclic bending behavior of hollow structural sections. *Journal of Constructional Steel Research*, **94**, 64-75.

[14] Flores Carreras CA, McCormick JP (2019): Relaxing Current Ductility Requirements in Tube-Based Seismic Moment Frames. *Proceedings of the 17th International Symposium on Tubular Structures*, 422-429.

[15] ASTM International (2018): Standard Specification for Cold-Formed Welded and Seamless Carbon Steel Structural Tubing in Rounds and Shapes. *ASTM A500/A500M-18*, West Conshohocken, Pennsylvania.

[16] AISC (2016): Seismic Provisions for Structural Steel Buildings. *ANSI/AISC 341-16*, Chicago, Illinois.

[17] Fadden M, McCormick J (2012): Cyclic Quasi-Static Testing of Hollow Structural Section Beam Members. *Journal of Structural Engineering*, **138**(5), 561-570.

